Molecular Cell
Short Article

Structure of the Endonuclease Domain of MutL: Unlicensed to Cut

Monica C. Pillon,[1] Jessica J. Lorenowicz,[1] Michael Uckelmann,[2] Andrew D. Klocko,[3] Ryan R. Mitchell,[1] Yu Seon Chung,[1] Paul Modrich,[4,5] Graham C. Walker,[6] Lyle A. Simmons,[3] Peter Friedhoff,[2] and Alba Guarné[1,*]
[1]Department of Biochemistry and Biomedical Sciences, McMaster University, Hamilton, ON L8N 3Z5, Canada
[2]Institut für Biochemie (FB 08), Justus-Liebig-Universität, D-35392 Giessen, Germany
[3]Department of Molecular, Cellular, and Developmental Biology, University of Michigan, Ann Arbor, MI 48103, USA
[4]Department of Biochemistry
[5]Howard Hughes Medical Institute
Duke University Medical Center, Durham, NC 27710, USA
[6]Department of Biology, Massachusetts Institute of Technology, Cambridge, MA 02139, USA
*Correspondence: guarnea@mcmaster.ca
DOI 10.1016/j.molcel.2010.06.027

SUMMARY

DNA mismatch repair corrects errors that have escaped polymerase proofreading, increasing replication fidelity 100- to 1000-fold in organisms ranging from bacteria to humans. The MutL protein plays a central role in mismatch repair by coordinating multiple protein-protein interactions that signal strand removal upon mismatch recognition by MutS. Here we report the crystal structure of the endonuclease domain of *Bacillus subtilis* MutL. The structure is organized in dimerization and regulatory subdomains connected by a helical lever spanning the conserved endonuclease motif. Additional conserved motifs cluster around the lever and define a Zn^{2+}-binding site that is critical for MutL function in vivo. The structure unveils a powerful inhibitory mechanism to prevent undesired nicking of newly replicated DNA and allows us to propose a model describing how the interaction with MutS and the processivity clamp could license the endonuclease activity of MutL. The structure also provides a molecular framework to propose and test additional roles of MutL in mismatch repair.

INTRODUCTION

DNA mismatch repair (MMR) maintains genomic stability by correcting errors that have escaped polymerase proofreading (Kunkel and Erie, 2005). MMR proteins are also implicated in a variety of other cellular processes such as DNA damage signaling, apoptosis, meiotic and mitotic recombination, and somatic hypermutation (Modrich, 2006). Mutations in MMR genes are associated with an increased mutation rate and microsatellite instability, the hallmark of human nonpolyposis colorectal cancer (Peltomaki, 2005).

Initiation of MMR depends on the coordinated action of three proteins. MutS recognizes a mismatched base pair or a small insertion/deletion loop and recruits MutL in an ATP-dependent manner. Subsequently, the newly synthesized strand is marked for repair. In *Escherichia coli*, strand discrimination is achieved by mismatch-provoked activation of the MutH endonuclease, which cleaves the unmethylated DNA strand at hemimethylated GATC sites transiently generated during DNA replication. Although most bacteria and all eukaryotes do not encode a MutH homolog, a pre-existing nick is sufficient to activate MMR in a system reconstituted from purified proteins (Zhang et al., 2005). It has been shown that MutL homologs from species lacking a MutH endonuclease harbor an intrinsic latent nicking endonuclease activity that is vital for its function in MMR (Erdeniz et al., 2007; Kadyrov et al., 2006, 2007, 2008).

MutL is composed of two structurally conserved domains connected by a variable flexible linker (Guarné et al., 2004). The N-terminal region encompasses an ATPase domain of the GHL ATPase superfamily that is conserved from bacteria to humans (Ban et al., 1999; Guarné et al., 2001). Conversely, the sequence conservation in the C-terminal dimerization region of MutL is low. The structure of the C-terminal domain of *E. coli* MutL (EcMutL) reveals that this region is organized into two distinct subdomains (Guarné et al., 2004; Kosinski et al., 2005).

While prokaryotic MutL homologs form homodimers, their eukaryotic counterparts form heterodimers. In humans, there are four paralogs of MutL (hMLH1, hPMS2, hPMS1, and hMLH3) that form three heterodimers by association of hMLH1 with hPMS2 (hMutLα), hPMS1 (hMutLβ), and hMLH3 (hMutLγ) (Li and Modrich, 1995; Lipkin et al., 2000; Raschle et al., 1999). hMutLα is necessary for MMR function, and hMutLγ has a role in meiotic recombination; however, the function of hMutLβ is unknown (Kunkel and Erie, 2005). The C-terminal regions of hPMS2 and hMLH3 encompass a conserved $DQHA(X)_2E(X)_4E$ motif that is required for endonuclease activity. Based on sequence analysis and molecular modeling, three additional conserved motifs (ACR, C[P/N]HGRP, and FXR) have been predicted to form a single active site with the endonuclease motif (Kosinski et al., 2008). Analysis of the reconstituted human MMR system indicates that the endonuclease activity of MutLα provides a loading site for MutSα-activated exonuclease I (Kadyrov et al., 2006).

Table 1. Data Collection and Refinement

Data Collection	Crystal Form I				Crystal Form II	Crystal Form III
Space Group	$C222_1$				$P2_12_12_1$	$P2_12_12_1$
Unit Cell (Å)	a = 88.3, b = 94.9, c = 218.7				a = 33.2, b = 74.6, c = 182.2	a = 33.2, b = 74.6, c = 182.2
Wavelength (Å)	0.9794 (Se-edge)	0.9792 (Se-peak)	0.9686 (Se-remote)	1.0809 (native)	1.282 (Zn-peak)	1.2796 (Zn-peak)
Resolution (Å)[a]	35-2.8 (2.9-2.8)	35-2.8 (2.9-2.8)	35-2.8 (2.9-2.8)	50-2.38 (2.47-2.38)	50-2.0 (2.03-2.00)	50-2.15 (2.19-2.15)
Completeness (%)[a]	98.2 (88.3)	98.6 (91.4)	92.5 (55.9)	95.9 (76.0)	100 (100)	99.3 (93.3)
Redundancy[a]	6.2 (5.0)	6.3 (5.4)	6.3 (3.9)	5.5 (4.5)	7.5 (7.4)	10.3 (6.3)
R_{merge} (%)[a]	6.5 (21.0)	8.1 (21.3)	7.2 (23.1)	4.0 (22.5)	8.3 (67.6)	8.9 (70.7)
$I/\sigma(I)$[a]	20.2 (6.9)	18.5 (5.6)	17.8 (4.9)	41.5 (4.5)	25.9 (3.1)	22.4 (2.3)
ASU content	Four monomers			Four monomers	One dimer	One dimer
Data Refinement						
Resolution (Å)				30–2.5	38.9–2.0	32.8–2.3
Reflections (work)				31,772	60,020	41,004
Reflections (test)				1,631	3,049	2,113
Atoms refined				6,122	3,294	3,120
Solvent atoms				105	190	74
Zn atoms				–	–	4
R (R_{free}) (%)				21.7 (26.8)	19.1 (22.8)	21.4 (26.9)
Rmsd in bonds (Å)				0.003	0.005	0.004
Rmsd in angles (°)				0.609	0.875	0.745
Mean B values (Å)				44.1	45.6	43.9

[a] Data in the highest-resolution shell are shown in parentheses.

Here we present the structure of the C-terminal dimerization domain of *Bacillus subtilis* MutL (BsMutL) harboring the endonuclease activity of the protein. The structure reveals the conserved three-dimensional organization of the endonuclease site of MutL and exposes the presence of a regulatory Zn^{2+}-binding site that is important for the MMR function of BsMutL in vivo. The structure allows for us to propose a model describing how the association of MutS and the DNA polymerase III processivity clamp (β clamp) with MutL could license nicking of a newly synthesized DNA strand.

RESULTS AND DISCUSSION

Crystal Structure of BsMutL-CTD

Three crystal forms of the C-terminal domain of BsMutL (BsMutL-CTD) were obtained. Crystal form I was used to determine the structure of BsMutL-CTD by multiwavelength anomalous diffraction using crystals grown with Sel-Met substituted protein (Table 1). This crystal includes four independent monomers (molecules A–D) in the asymmetric unit that associate through crystal symmetry to form the functional BsMutL-CTD dimer. Crystal forms II and III contained a single dimer in the asymmetric unit. In the three structures, the N- and C-terminal ends of BsMutL-CTD (residues 433–461/580–627) define the dimerization subdomain, while residues 474–573 define an external subdomain that protrudes to the solvent, herein referred to as the regulatory subdomain (Figures 1A and 1B). The subdomains are connected by helix αA (residues 463–473), encompassing the conserved endonuclease motif, and the linker connecting helices αD-αE (residues 575–581), which is disordered in our structures (Figure 1A). However, the relative orientation between subdomains varies from one crystal form to another (see Movie S1 available online).

The three complimentary conserved motifs associate with the endonuclease motif cluster around helix αA to delineate a single catalytic site with the conserved endonuclease motif (^{462}DQHA(X)$_2$E(X)$_4$E) (Figures 1B and 1C). ^{604}CPHGRP resides in the αE-β8 loop, ^{572}SCK (consensus sequence ACR) is the last turn of the αD helix, and ^{623}FKR, at the C terminus of the protein, reaches the active site of the other protomer (Figure 1B). Except for the ^{572}SCK motif, contributed by the regulatory subdomain, all motifs reside in the dimerization subdomain.

Two additional conserved motifs have been identified within the C-terminal region of MutLα (Kosinski et al., 2008). The ^{443}GQ motif resides on the β1 strand of the dimerization subdomain. This strand is in the vicinity of the αD-αE loop and hence it may indirectly contribute to the overall stability of the active site. The ^{487}QEMIVP motif (consensus sequence QXLLXP) is on the surface of the regulatory subdomain and conspicuously exposed to the solvent (Figure 1B). Conservation of the QXLLXP motif is not correlated with the endonuclease activity of MutL, suggesting that it could mediate the interaction with other repair factors.

Even though the C-terminal regions of EcMutL and BsMutL have very low sequence similarity, their structures have nearly identical topologies (Figure S1). However, key differences exist. Superimposition of the EcMutL-CTD monomer onto the BsMutL-CTD monomer returned root-mean-square deviations (rmsds) of only 1 Å for the dimerization subdomains but >2 Å for the

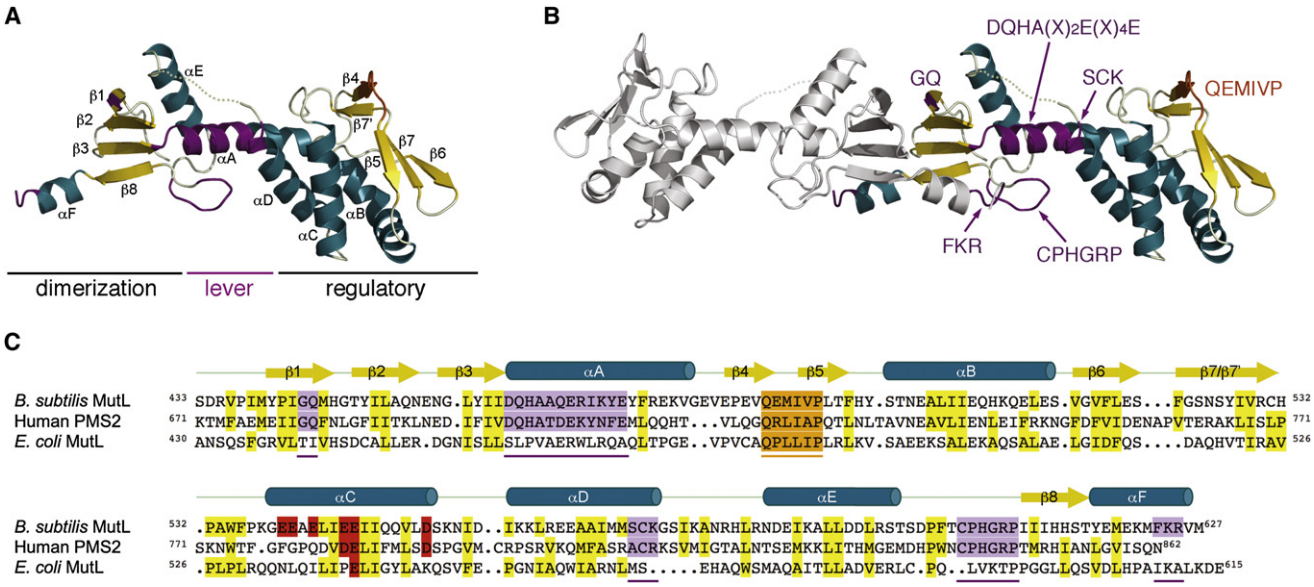

Figure 1. Crystal Structure of BsMutL-CTD

(A) Ribbon diagram of the BsMutL-CTD monomer. Secondary structure motifs are labeled and colored blue (helices) and yellow (strands) with the connecting loops in light green. The endonuclease and the endonuclease-associated motifs are shown in purple, while the additional conserved motifs are shown in orange.

(B) Ribbon diagram of the BsMutL-CTD dimer with one protomer shown as in (A) and the other one as gray ribbons.

(C) Sequence alignment of the C-terminal regions of BsMutL, hPMS2, and EcMutL. Secondary structure elements of BsMutL-CTD are shown as arrows (strands) and cylinders (helices). The five conserved motifs are highlighted in purple and underlined. Conserved hydrophobic residues are highlighted in yellow. The conserved ^{487}QEMIVP motif is highlighted in orange. See also Figure S1.

regulatory subdomains, reflecting the increased divergence of this region. This is intriguing because the regulatory subdomain contributes minimally to the endonuclease site. The most striking difference between the two structures is the organization of the secondary structure elements surrounding helix αA, which would preclude the formation of a functional endonuclease site even if EcMutL had the conserved DQHA(X)$_2$E(X)$_4$E motif (Figure S1). Notably, the extended αE-β8 loop in BsMutL, rather than the additional helix seen in EcMutL, brings the ^{604}CPHGRP motif closer to helix αA and secludes the endonuclease site. The dimerization interfaces are also remarkably different. While the BsMutL dimer buries 1065 Å^2, the EcMutL dimer only conceals 910 Å^2. Interestingly, the reorientation of the apposing β sheets in the BsMutL-CTD dimer allows the ^{623}FKR motif to reach the adjacent endonuclease site.

BsMutL Has Weak Endonuclease Activity

Similarly to other MutL orthologs, BsMutL had a weak endonuclease activity dependent on Mn^{2+} (Figure 2A). Both a point mutation in the endonuclease motif (D462N) and deletion of the ATPase domain virtually abolished the endonuclease activity of BsMutL (Figure 2A). This finding is interesting in light of the recent experiments revealing that the C-terminal domains of *Neisseria ghonorrhoeae* and *Aquifex aeolicus* have endonuclease activity (Duppatla et al., 2009; Mauris and Evans, 2009). However, the specific activity of AaeMutL-CTD is much lower than that of the full-length protein. We suspected that the lack of nicking activity by BsMutL-CTD could be due to a DNA-binding defect, since EcMutL-CTD does not bind DNA stably (Guarné et al., 2004). Indeed, BsMutL-CTD did not bind supercoiled DNA, while other variants of BsMutL did (Figure 2C).

Addition of 0.5 mM ATP stimulated the nicking activity of BsMutL, but higher concentrations of ATP (5 mM) inhibited the nicking activity, presumably due to excess nucleotide chelating Mn^{2+} ions away (Figure 2B, lanes 5 and 6). Unexpectedly, addition of ATP and/or Mg^{2+} stimulated a second cut on the nicked DNA to yield a linear product. The cut of the two strands at nearby points could be due to the presence of two endonuclease sites in the BsMutL homodimer or a consequence of the high-ion concentrations used in the experiment. We favor the former because incubation with 10 mM Mn^{2+} did not cause nicking of the two strands (data not shown), but addition of only 1 mM of a second metal ion such as Zn^{2+} or Co^{2+} yielded a linear product (Figure 2D). Interestingly, Mg^{2+} did not support double nicking under these conditions, suggesting that BsMutL may have higher affinity for Zn^{2+} or Co^{2+} than Mg^{2+}.

We then characterized the ATPase activity of BsMutL (K_m = 0.4 mM and k_{cat} = 0.3 min^{-1}) and found that it is a weaker ATPase than other MutL homologs (Ban et al., 1999; Guarné et al., 2001; Hall et al., 2002). Given the slow ATP-hydrolysis rate, the stimulation of the endonuclease activity of BsMutL was likely due to ATP binding rather than ATP hydrolysis. In good agreement with this idea, ADP did not stimulate the endonuclease activity of BsMutL (Figure 2B, lanes 9 and 10). However, two known nonhydrolyzable analogs of ATP, AMPPnP and ATPγS, did not stimulate the endonuclease activity of BsMutL beyond the levels observed when both Mn^{2+} and Mg^{2+} were present (Figure 2B, compare lanes 4, 7, 9, and 11).

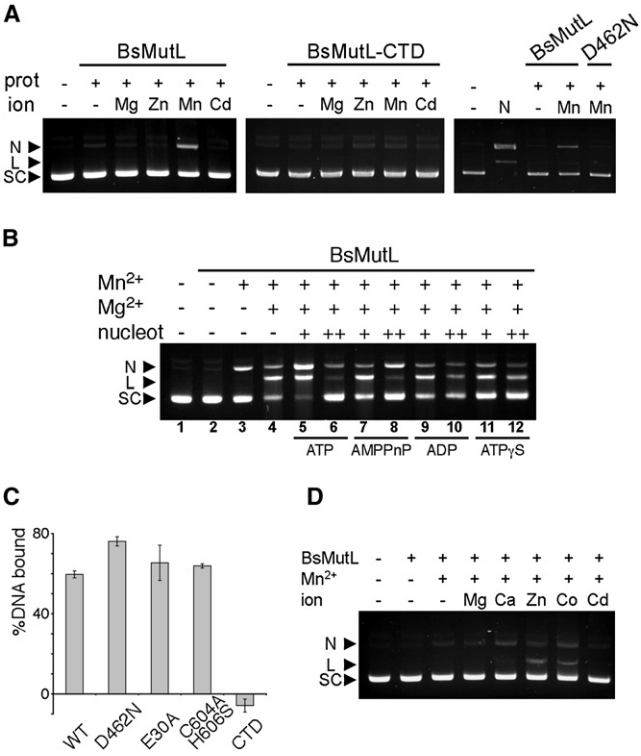

Figure 2. Endonuclease Activity of BsMutL

(A) Nicking activity of BsMutL (left) and BsMutL-CTD (center) in the presence of Mg^{2+}, Zn^{2+}, Mn^{2+}, or Cd^{2+} as indicated. Comparison of the nicking activity of BsMutL and BsMutL-D462N in the presence of Mn^{2+} (right). Migration of supercoiled (SC), nicked (N), and linear (L) DNA is indicated.

(B) Endonuclease activity of BsMutL in the presence of 0.5 mM (+) and 5 mM (++) nucleotide.

(C) DNA binding by BsMutL (WT), BsMutL-CTD (CTD), and BsMutL variants as indicated. Data are presented as the mean of three independent measurements, and the error bars correspond to the standard errors of the mean (SEM = $\sigma/\sqrt{n}$, where σ is the average and n the sample size).

(D) Stimulation of the endonuclease activity of BsMutL (1 mM Mn^{2+}) by a second divalent metal ion (1 mM).

Conceivably, the ATP-dependent stimulation of the endonuclease activity of BsMutL could be due to a conformational change induced by ATP binding as seen in other MutL orthologs (Ban et al., 1999; Sacho et al., 2008), which would bring DNA bound at the ATPase domain in close proximity to the endonuclease site. If this is the case, our results suggest that only ATP can induce efficiently such conformational change.

BsMutL Has a Regulatory Zn^{2+}-Binding Site

Although the endonuclease activity of BsMutL was metal dependent and the conserved motifs around helix αA define a putative Zn^{2+}-binding site (Kosinski et al., 2008), no metal ions were found in the BsMutL-CTD structure (crystal form I). However, different crystal forms were obtained when the protein storage buffer (crystal form II) and the crystallization solution (crystal form III) were supplemented with $ZnCl_2$. While the ^{462}DQHA(X)$_2$E(X)$_4$E, ^{572}SCK, and ^{604}C(P/N)HGRP motifs were much closer in crystal form II than crystal form I, no metal was found in this crystal form either. Conversely, the BsMutL-CTD dimer found in the asymmetric unit of crystal form III contained two Zn^{2+} ions bound to each protomer; a fully occupied Zn^{2+} ion (Zn^{2+}A) was coordinated by the side chains of residues Glu468, Cys604, His606, and a well-ordered water molecule, and a partly occupied site (Zn^{2+}B) coordinated by the side chains of residues His464, Glu468, Cys573 and a water molecule (Figure 3A). The nature of the metal ion was confirmed on the anomalous difference electron density maps from diffraction data collected at the Zn^{2+} absorption edge (Table 1).

It had been previously reported that the putative Zn^{2+}-binding site in hPMS2 could be related to the regulatory metal-binding site found in the iron-dependent repressors from the DtxR/MntR family (Kosinski et al., 2008). A structural comparison revealed that, while motifs ^{462}DQHAX$_2$EX$_4$E, ^{572}SCK, and ^{604}CPHGRP from BsMutL could be superimposed to the regulatory metal-binding sites of IdeR or MntR, the residues coordinating the metal ion differed. However, another Mn^{2+}-dependent repressor from the same family (ScaR, PDB 3HRU) encompasses a regulatory metal-binding site identical to the fully occupied Zn^{2+} site in BsMutL-CTD.

To probe whether the two metal-bound sites found in our structure were true Zn^{2+}-binding sites, we measured the affinity of purified BsMutL-CTD and various BsMutL-CTD variants for zinc. To this end, we measured the fluorescence of increasing concentrations of Zn^{2+} bound to the fluorescence indicator FluoZin-3. In the absence of protein, fluorescence increased exponentially, reaching maximum values at around 1.5–2 μM $ZnCl_2$. The sigmoidal response observed for wild-type and the D462N, H464S, and E473K variants was characteristic of zinc binding by the protein (Figure 3B), suggesting that these BsMutL-CTD variants still retained the ability to bind zinc. Addition of the sulfhydryl-modifying agent methyl methanethiosulfonate (MMTS) resulted in an increase of fluorescence to the level detected in the absence of protein, indicating that one or more cysteine residues within the C-terminal domain of BsMutL were important for Zn^{2+} binding (data not shown). Conversely, fluorescence profiles of E468K, C604A, H606S, and C604A/H606S mutants did not have a sigmoidal response (Figure 3B), revealing that these BsMutL-CTD variants had lost the ability to bind zinc. These results confirmed that Glu468, Cys604, and His606 define the Zn^{2+}-binding site in BsMutL (Figure 3A).

Integrity of the Conserved Motifs Is Important for Mismatch Repair In Vivo

We presumed that the integrity of the Zn^{2+}-binding site in MutL would be important for proper MMR. Therefore, we measured the MMR efficiency of BsMutL variants encompassing point mutations in the conserved residues involved in the endonuclease or Zn^{2+}-binding sites. Mutation of D462A, H464A, E468K, or H606A completely inactivated MMR in vivo (Figure 3C), underscoring the importance of these residues. Similarly, the equivalent mutations in hPMS2 also conferred a strong mutator phenotype (Kosinski et al., 2008). Conversely, the BsMutL-Q463A and BsMutL-E473K variants had similar MMR efficiency to wild-type BsMutL, suggesting that not all the conserved residues within these motifs play essential roles in MMR.

We next analyzed the importance of other conserved motifs found in the C-terminal region of MutL, namely the ^{487}QEMIVP

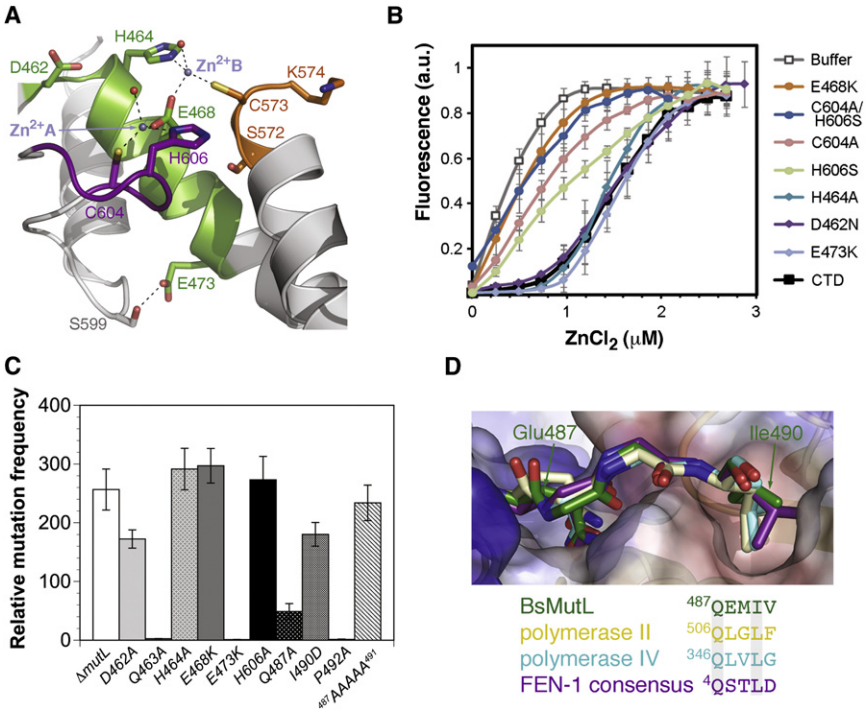

Figure 3. Regulatory Zn^{2+}-Binding Site in BsMutL-CTD

(A) Organization of the endonuclease site of BsMutL-CTD bound to Zn^{2+} (crystal form III). Hydrogen bonds are shown as black dashed lines with the water molecules and Zn^{2+} ions shown as red and lilac spheres, respectively. Conserved motifs are color coded green ($^{462}DQHAX_2EX_4E$), purple ($^{604}CPHGRP$), and orange (^{572}SCK).

(B) Zinc-affinity profiles of BsMutL-CTD and point mutants of BsMutL-CTD as indicated. Data are presented as the mean of three independent measurements ± SEM.

(C) Bar diagram showing the relative mutation frequency of the indicated *mutL* variants altered in the Zn^{2+}-binding, the endonuclease site, and the putative β-binding motif. Data are presented as the mean of four independent cultures ±SEM.

(D) Superimposition of the β-binding motif in BsMutL-CTD (green) onto those of Pol II (yellow, PDB 3D1E), Pol IV (cyan, PDB 1UNN), and FEN-1 (purple, PDB 1RXM) shown as a main-chain trace with the β clamp structure (PDB 3D1E) presented as a semitransparent electrostatic potential surface. See also Figures S2 and S3 and Movie S1.

motif. Mutation of Ile490 almost completely inactivated MMR in vivo, whereas mutation of Pro492 was without effect (Figure 3C). A BsMutL-Q487A variant conferred approximately a 50-fold mutator phenotype about 5-fold lower than a *mutL* null strain. Replacement of residues ^{487}QEMIV with five alanine residues also abrogated MMR in vivo (Figure 3C). This conserved loop is conspicuously exposed and loosely resembles the consensus β-binding motif (Dalrymple et al., 2001). Most notably, its conformation is nearly identical to that seen in the structures of other peptides bound to the β clamp (Figure 3D). Superimposition of the ^{486}VQEMIVPL sequence from BsMutL onto the structures of β clamp bound to peptides from polymerase II, FEN-1, and polymerase IV returned rmsds smaller than 0.5 Å. Accordingly, the regulatory subdomains of both BsMutL and EcMutL could be directly docked onto the structure of the *E. coli* β clamp. Interestingly, docking of the MutL-CTD dimer suggests that the interaction of one protomer would prevent the interaction of the other due to steric hindrance (Figure S2), suggesting a possible regulatory role for this interaction.

A Model for the Activation of the Endonuclease Activity

Based on the structures of BsMutL-CTD, we suggest that the conserved motifs in MutL define an endonuclease active site with two distinct subsites: a structural Zn^{2+}-binding site defined by the side chains of Glu468, Cys604, and His606; and a catalytic site likely defined by Asp462 and His464. Metal binding at the structural site locks the orientation between the dimerization and regulatory subdomains, which is highly variable in the absence of metal (Movie S1). Based on the three-dimensional organization of Asp462 and His464, the catalytic subsite could coordinate one or two metal ions to nick DNA (Yang, 2008). Supporting this idea, double-stranded DNA could be modeled onto the structure of BsMutL-CTD with the scissile bond at a distance compatible with catalysis activated by Asp462 and the adjacent 3′ phosphate providing the fourth coordination ligand of the regulatory Zn^{2+} ion (Figure S3).

In the context of the replication fork, the endonuclease activity of MutL ought to be repressed until a mismatch is encountered. A look at the electrostatic potential surface of BsMutL-CTD reveals a powerful suppression mechanism of DNA binding. The regulatory subdomain is covered with negative charges that guard the endonuclease site (Figure 4A). This could be a widely spread repression mechanism, since some of the negatively charged residues in helix αC are conserved in other MutL homologs harboring the endonuclease motif (Figure 1C and Kosinski et al., 2008). Licensing the endonuclease activity of MutL would thus require a significant conformational change or the interaction with other repair factors to overcome the DNA repulsion in the vicinity of the endonuclease site. We presume that a conformational change like that induced in MutLα upon nucleotide binding could allow DNA bound at the ATPase domain to reach the endonuclease site (Sacho et al., 2008). However, additional repair factors are likely required to mask helix αC.

The endonuclease activity of MutLα is greatly stimulated by the presence of PCNA and RFC (Kadyrov et al., 2006; Kadyrov et al., 2007), the eukaryotic homologs of the β clamp and the clamp loader. Additionally, MutSα and PCNA form a stable complex (Iyer et al., 2008). Human MutLα interacts with MutSα through its ATPase domain (Plotz et al., 2006), but the region of MutSα that interacts with MutLα is not known. Conceivably, the three proteins could form a ternary complex involved in strand discrimination; however, whether MutSα and MutLα can interact simultaneously with PCNA is controversial (Dzantiev et al., 2004; Lee and Alani, 2006). Bacterial MutS has two binding

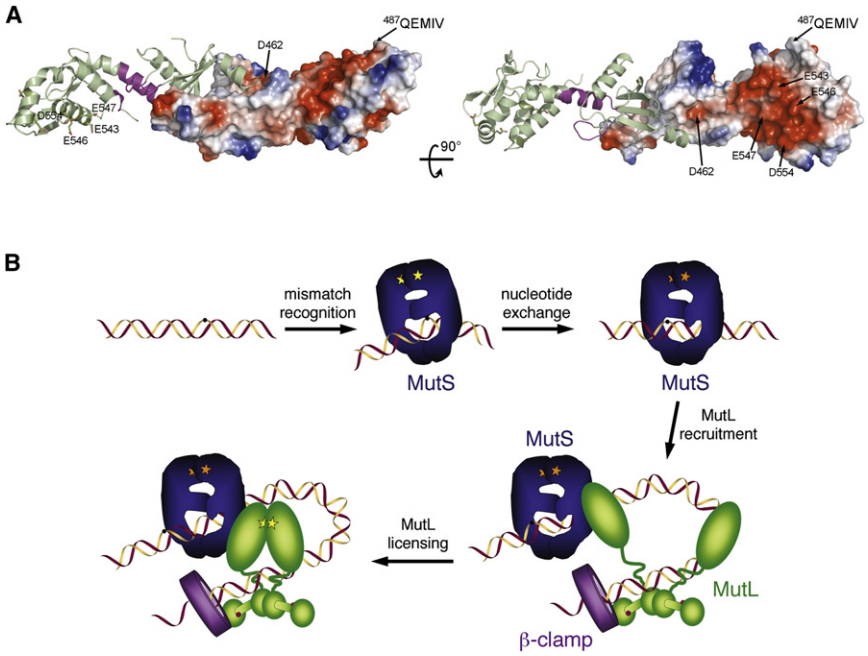

Figure 4. Model of Activation of the Endonuclease Activity of MutL

(A) Orthogonal views of the electrostatic surface potential of the BsMutL-CTD protomer. The second protomer is shown as a ribbon diagram with the endonuclease motifs in purple.

(B) Upon mismatch binding, MutS (blue) undergoes a nucleotide-dependent conformational change that triggers recruitment of MutL (green) to the mismatch site, likely aided by the β clamp (purple). ATP binding by MutL then promotes the association of its two ATPase subunits and brings the ATPase in close proximity to the dimerization domain of the protein. Coordinated interaction of MutS and β clamp bound to DNA (ribbon diagram) with ATP-bound MutL could thus license the latent endonuclease activity of MutL. ATP and ADP are shown as yellow and orange stars, respectively.

sites for the β clamp (Lopez de Saro et al., 2006; Simmons et al., 2008). In *B. subtilis*, the C-terminal site is necessary to recruit MutL to mismatches and to activate the MMR response (Simmons et al., 2008). We presume that the ATPase domain of MutL could interact with MutS, while its C-terminal domain interacts with the β clamp (Figure 4B). This model is supported by the presence of the β-binding-like motif (^{487}QEMIV) within the C-terminal domain of MutL and the fact that a PCNA-binding sequence has been identified in the dimerization region of yeast MLH1 (Lee and Alani, 2006).

Collectively, our data pose an attractive model in which the endonuclease activity of MutL is repressed by impaired DNA binding. Based on these data, the simplest mechanism would harness MutL and β clamp, allowing for DNA binding and licensing of the endonuclease activity. Consequently, the structure provides a platform for future mechanistic studies of MutL-MutS-β at the early steps of MMR.

EXPERIMENTAL PROCEDURES

Cloning, Purification, and Crystallization

Full-length BsMutL was amplified from genomic DNA and cloned into the pProEXHTa expression vector (Life Technologies). His-tagged BsMutL was purified using a Ni^{2+}-chelating affinity column equilibrated with 20 mM Tris (pH 8), 0.5 M NaCl, 1.4 mM β-mercaptoethanol, 5% glycerol, and 100 mM PMSF. BsMutL was eluted using 300 mM imidazole and subsequently injected on a hydrophobic column equilibrated with 20 mM Tris (pH 8), 1 M KCl, 1 mM DTT, and 5% glycerol. BsMutL was further purified by ionic exchange and size exclusion chromatography (MonoQ 5/50 and Superdex-S200, GE Healthcare) equilibrated with 20 mM Tris (pH 8), 100 mM KCl, 1 mM DTT, and 5% glycerol (storage buffer). Guided by a structure-based sequence alignment, we subcloned the C-terminal fragment of BsMutL (BsMutL-CTD, residues 433–627). BsMutL-CTD was purified similarly to BsMutL with an additional ionic exchange purification step after His-tag cleavage with TEV-protease. Mutants of BsMutL and BsMutL-CTD were generated by QuikChange (Stratagene) and verified by DNA sequencing (MOBIX, McMaster University).

Crystal form I was grown in 25% PEG-monomethyl ether 550, 0.1 M $MgCl_2$, 0.1 M Tris (pH 9), and 5% PEG 400. Two additional crystal forms were obtained when the protein was supplemented with 50 nM $ZnCl_2$ and 50 nM $CoCl_2$. Crystal form II was grown in 25% PEG 3350, 0.15–0.2 M NaCl, and 0.1 M Tris (pH 7). Addition of 0.5 mM $ZnCl_2$ to this crystallization solution yielded crystal form III. PEG 400 (10%) was added to all crystallization conditions prior to flash freezing in liquid nitrogen.

Data Collection and Structure Determination

For crystal form I, a three-wavelength MAD data set was collected at X29B in NSLS, Brookhaven National Laboratory (Upton, NY). Data were indexed, processed, and merged using HKL2000 (Otwinowski and Minor, 1997). Twenty-seven out of thirty-six Selenium sites were found and refined using SOLVE (Terwilliger and Berendzen, 1999). A native data set to 2.5 Å was used for subsequent manual building and refinement, which was done using standard protocols in phenix.refine and COOT (Afonine et al., 2005; Emsley and Cowtan, 2004). Complete data sets of crystal forms II and III were collected at the X25 beamline in NSLS. Data were collected at a wavelength corresponding to the Zn^{2+}-absorption edge (Table 1), as measured using fluorescence scans. All final models have more than 92% of the residues within the most favored regions in the Ramachandran plot and none in disallowed regions. Figures depicting molecular structures were generated using PyMol (DeLano, 2002).

Endonuclease and DNA-Binding Assays

BsMutL nicking activity was assayed as previously described (Kadyrov et al., 2006), with minor modifications described in the Supplemental Information. To assess DNA binding by BsMutL, supercoiled DNA (5 nM) was incubated with BsMutL variants (100 nM, dimer) in endonuclease buffer for 90 min at 37°C. Reaction mixtures (20 μL) were resolved on 1% TAE agarose gels and quantified using ImageJ (http://rsbweb.nih.gov/ij/). Data were presented as the mean of three independent measurements, and the error bars correspond to the standard errors of the mean (SEM = $\sigma/\sqrt{n}$, where σ is the average and n the sample size).

Zinc-Affinity Fluorescence Assay

Wild-type and variants of BsMutL-CTD (2 μM) were incubated with 1 μM FluoZin-3 (Invitrogen) in 10 mM HEPES (pH 6) and 200 mM KCl buffer treated with 1% Chelex-100 (Fluka). A calibration fluorescence curve was generated using buffer including increasing concentrations of $ZnCl_2$ (0.25–3 μM) in the absence of protein. Spectra (500–600 nm) were recorded at an excitation wavelength of 494 nm (corrected for buffer effects). Innerfilter effects were neglected because a linear fluorescence intensity response up to stoichiometric amounts

of Zn^{2+} was seen when using 4 μM FluoZin-3. Data were presented as the mean of three independent measurements, and the error bars correspond to the SEM.

Mismatch Repair Assays of BsMutL Variants

MMR assays were performed largely as described (Simmons et al., 2008). See the Supplemental Information for a more complete description of the methods.

ACCESSION NUMBERS

Atomic coordinates and structure factors of BsMutL-CTD have been deposited in the Protein Data Bank under accession codes 3GAB, 3KDG, and 3KDK.

SUPPLEMENTAL INFORMATION

Supplemental Information includes Supplemental Experimental Procedures, three figures, one movie, and one table and can be found with this article at doi:10.1016/j.molcel.2010.06.027.

ACKNOWLEDGMENTS

We thank Michael d'Elia, Pablo Romero, and the staff at the Brookhaven National Laboratory for technical assistance. We are grateful to Drs. Murray Junop and Joaquin Ortega for critical reading of the manuscript. This work was supported by the National Sciences and Engineering Research Council of Canada (NSERC, 288295 to A.G.), the German Science Foundation (FR-1495/4-1 to P.F.), start-up funds from the University of Michigan (to L.A.S.), and the National Institutes of Health (CA21615 to G.C.W. and GM45190 to P.M.). M.C.P. is supported by an NSERC scholarship, and G.C.W. is an American Cancer Society Research Professor.

Received: January 15, 2010
Revised: April 5, 2010
Accepted: May 12, 2010
Published: July 8, 2010

REFERENCES

Afonine, P.V., Grosse-Kunstleve, R.W., and Adams, P.D. (2005). phenix.refine. CCP4 Newsletter *42*, contribution 8.

Ban, C., Junop, M., and Yang, W. (1999). Transformation of MutL by ATP binding and hydrolysis: a switch in DNA mismatch repair. Cell *97*, 85–97.

Dalrymple, B.P., Kongsuwan, K., Wijffels, G., Dixon, N.E., and Jennings, P.A. (2001). A universal protein-protein interaction motif in the eubacterial DNA replication and repair systems. Proc. Natl. Acad. Sci. USA *98*, 11627–11632.

DeLano, W.L. (2002). The PyMOL Molecular Graphic Systems (Palo Alto, CA: DeLano Scientific).

Duppatla, V., Bodda, C., Urbanke, C., Friedhoff, P., and Rao, D.N. (2009). The C-terminal domain is sufficient for endonuclease activity of Neisseria gonorrhoeae MutL. Biochem. J. *423*, 265–277.

Dzantiev, L., Constantin, N., Genschel, J., Iyer, R.R., Burgers, P.M., and Modrich, P. (2004). A defined human system that supports bidirectional mismatch-provoked excision. Mol. Cell *15*, 31–41.

Emsley, P., and Cowtan, K. (2004). Coot: model-building tools for molecular graphics. Acta Crystallogr. D Biol. Crystallogr. *60*, 2126–2132.

Erdeniz, N., Nguyen, M., Deschenes, S.M., and Liskay, R.M. (2007). Mutations affecting a putative MutLalpha endonuclease motif impact multiple mismatch repair functions. DNA Repair (Amst.) *6*, 1463–1470.

Guarné, A., Junop, M.S., and Yang, W. (2001). Structure and function of the N-terminal 40 kDa fragment of human PMS2: a monomeric GHL ATPase. EMBO J. *20*, 5521–5531.

Guarné, A., Ramon-Maiques, S., Wolff, E.M., Ghirlando, R., Hu, X., Miller, J.H., and Yang, W. (2004). Structure of the MutL C-terminal domain: a model of intact MutL and its roles in mismatch repair. EMBO J. *23*, 4134–4145.

Hall, M.C., Shcherbakova, P.V., and Kunkel, T.A. (2002). Differential ATP binding and intrinsic ATP hydrolysis by amino-terminal domains of the yeast Mlh1 and Pms1 proteins. J. Biol. Chem. *277*, 3673–3679.

Iyer, R.R., Pohlhaus, T.J., Chen, S., Hura, G.L., Dzantiev, L., Beese, L.S., and Modrich, P. (2008). The MutSalpha-proliferating cell nuclear antigen interaction in human DNA mismatch repair. J. Biol. Chem. *283*, 13310–13319.

Kadyrov, F.A., Dzantiev, L., Constantin, N., and Modrich, P. (2006). Endonucleolytic function of MutLalpha in human mismatch repair. Cell *126*, 297–308.

Kadyrov, F.A., Holmes, S.F., Arana, M.E., Lukianova, O.A., O'Donnell, M., Kunkel, T.A., and Modrich, P. (2007). Saccharomyces cerevisiae MutLa is a mismatch repair endonuclease. J. Biol. Chem. *282*, 37181–37190.

Kosinski, J., Steindorf, I., Bujnicki, J.M., Giron-Monzon, L., and Friedhoff, P. (2005). Analysis of the quaternary structure of the MutL C-terminal domain. J. Mol. Biol. *351*, 895–909.

Kosinski, J., Plotz, G., Guarné, A., Bujnicki, J.M., and Friedhoff, P. (2008). The PMS2 subunit of human MutLalpha contains a metal ion binding domain of the iron-dependent repressor protein family. J. Mol. Biol. *382*, 610–627.

Kunkel, T.A., and Erie, D.A. (2005). DNA mismatch repair. Annu. Rev. Biochem. *74*, 681–710.

Lee, S.D., and Alani, E. (2006). Analysis of interactions between mismatch repair initiation factors and the replication processivity factor PCNA. J. Mol. Biol. *355*, 175–184.

Li, G.M., and Modrich, P. (1995). Restoration of mismatch repair to nuclear extracts of H6 colorectal tumor cells by a heterodimer of human MutL homologs. Proc. Natl. Acad. Sci. USA *92*, 1950–1954.

Lipkin, S.M., Wang, V., Jacoby, R., Banerjee-Basu, S., Baxevanis, A.D., Lynch, H.T., Elliott, R.M., and Collins, F.S. (2000). MLH3: a DNA mismatch repair gene associated with mammalian microsatellite instability. Nat. Genet. *24*, 27–35.

Lopez de Saro, F.J., Marinus, M.G., Modrich, P., and O'Donnell, M. (2006). The beta sliding clamp binds to multiple sites within MutL and MutS. J. Biol. Chem. *281*, 14340–14349.

Mauris, J., and Evans, T.C. (2009). Adenosine triphosphate stimulates Aquifex aeolicus MutL endonuclease activity. PLoS ONE *4*, e7175. 10.1371/journal.pone.0007175.

Modrich, P. (2006). Mechanisms in eukaryotic mismatch repair. J. Biol. Chem. *281*, 30305–30309.

Otwinowski, Z., and Minor, W. (1997). Processing of X-ray diffraction data collected in oscillation mode. In Methods in Enzymology, C.W. Carter and R.M. Sweet, eds. (New York: Academic Press), pp. 307–326.

Peltomaki, P. (2005). Lynch syndrome genes. Fam. Cancer *4*, 227–232.

Plotz, G., Welsch, C., Giron-Monzon, L., Friedhoff, P., Albrecht, M., Piiper, A., Biondi, R.M., Lengauer, T., Zeuzem, S., and Raedle, J. (2006). Mutations in the MutSalpha interaction interface of MLH1 can abolish DNA mismatch repair. Nucleic Acids Res. *34*, 6574–6586.

Raschle, M., Marra, G., Nystrom-Lahti, M., Schar, P., and Jiricny, J. (1999). Identification of hMutLbeta, a heterodimer of hMLH1 and hPMS1. J. Biol. Chem. *274*, 32368–32375.

Sacho, E.J., Kadyrov, F.A., Modrich, P., Kunkel, T.A., and Erie, D.A. (2008). Direct visualization of asymmetric adenine-nucleotide-induced conformational changes in MutL alpha. Mol. Cell *29*, 112–121.

Simmons, L.A., Davies, B.W., Grossman, A.D., and Walker, G.C. (2008). Beta clamp directs localization of mismatch repair in Bacillus subtilis. Mol. Cell *29*, 291–301.

Terwilliger, T.C., and Berendzen, J. (1999). Automated structure solution for MIR and MAD. Acta Crystallogr. D. Biol. Crystallogr. *55*, 849–861.

Yang, W. (2008). An equivalent metal ion in one- and two-metal-ion catalysis. Nat. Struct. Mol. Biol. *15*, 1228–1231.

Zhang, Y., Yuan, F., Presnell, S.R., Tian, K., Gao, Y., Tomkinson, A.E., Gu, L., and Li, G.M. (2005). Reconstitution of 5′-directed human mismatch repair in a purified system. Cell *122*, 693–705.